Medical Engineering and Physics 64 (2019) 1–6

Contents lists available at ScienceDirect

Medical Engineering and Physics

journal homepage: www.elsevier.com/locate/medengphy

Dual-mode artificially-intelligent diagnosis of breast tumours in shear-wave elastography and B-mode ultrasound using deep polynomial networks

Qi Zhang[a,b,*], Shuang Song[a,b], Yang Xiao[c,**], Shuai Chen[a,b], Jun Shi[a], Hairong Zheng[c]

[a] Shanghai Institute for Advanced Communication and Data Science, Shanghai University, Room 803, Xiangying Building, No. 333, Nanchen Road, Shanghai 200444, China
[b] The SMART (Smart Medicine and AI-based Radiology Technology) Lab, Institute of Biomedical Engineering, Shanghai University, Shanghai 200444, China
[c] Paul C. Lauterbur Research Center for Biomedical Imaging, Institute of Biomedical and Health Engineering, Shenzhen Institutes of Advanced Technology, Chinese Academy of Sciences, 1068 Xueyuan Ave., SZ University Town, Shenzhen 518055, China

ARTICLE INFO

Article history:
Received 30 July 2018
Revised 21 November 2018
Accepted 4 December 2018

Keywords:
Dual-modal diagnosis
Shear-wave elastography
B-mode ultrasound
Breast tumor
Artificial intelligence
Deep polynomial network

ABSTRACT

The main goal of this study is to build an artificial intelligence (AI) architecture for automated extraction of dual-modal image features from both shear-wave elastography (SWE) and B-mode ultrasound, and to evaluate the AI architecture for classification between benign and malignant breast tumors. In this AI architecture, ultrasound images were segmented by the reaction diffusion level set model combined with the Gabor-based anisotropic diffusion algorithm. Then morphological features and texture features were extracted from SWE and B-mode ultrasound images at the contourlet domain. Finally, we employed a framework for feature learning and classification with the deep polynomial network (DPN) on dual-modal features to distinguish between malignant and benign breast tumors. With the leave-one-out cross validation, the DPN method on dual-modal features achieved a sensitivity of 97.8%, a specificity of 94.1%, an accuracy of 95.6%, a Youden's index of 91.9% and an area under the receiver operating characteristic curve of 0.961, which was superior to the classic single-modal methods, and the dual-modal methods using the principal component analysis and multiple kernel learning. These results have demonstrated that the dual-modal AI-based technique with DPN has the potential for breast tumor classification in future clinical practice.

1. Introduction

Breast cancer is the most common cancer in women and has high mortality of 508 000 annually [1,2]. The early diagnosis of patients with breast cancer is crucial to improve the prognosis of patients and prolong their survival [3]. It is of great value to differentiate between benign and malignant breast tumors for the diagnosis and treatment of breast cancer. At present, there are two main diagnostic methods for diagnosis of breast cancer: pathology and imaging. Pathology is the gold standard for diagnosis of breast cancer. However, it is invasive and thus is not suitable for breast screening [4].

Ultrasound imaging technology has been recognized as the main method for early diagnosis of breast cancer because of its non-ionizing, non-invasive, and low-cost nature, as well as its capability of real-time dynamic imaging and imaging of dense breast tissue [5]. Traditional ultrasound imaging such as B-mode ultrasound provides useful information pertaining the number, size, shape and boundary of a breast tumor [6,7]. Shear-wave elastography (SWE) has emerged as an effective imaging tool for measurement of breast tissue elasticity and early detection of breast cancer based on the fact that the change of breast tissue elasticity may be earlier than its morphological changes [8].

The SWE imaging system often provides dual-modal visualization of breast tumors consisting of both a B-mode image and an elastogram. However, the current diagnosis methods for differentiating benign and malignant breast tumors mainly use single modality, either B-mode or elastography, and combination of dual modalities for diagnosis is limited. In this paper, we focus on dual-modal discrimination between benign and malignant breast tumors by combining complementary diagnostic information provided by SWE and B-mode [9].

* Corresponding author at: Shanghai Institute for Advanced Communication and Data Science, Shanghai University, Room 803, Xiangying Building, No. 333, Nanchen Road, Shanghai 200444, China.
** Corresponding author at: Shenzhen Institutes of Advanced Technology, Chinese Academy of Sciences, 1068 Xueyuan Ave., SZ University Town, Shenzhen 518055, China.
E-mail addresses: zhangq@t.shu.edu.cn (Q. Zhang), yang.xiao@siat.ac.cn (Y. Xiao).

https://doi.org/10.1016/j.medengphy.2018.12.005
1350-4533/

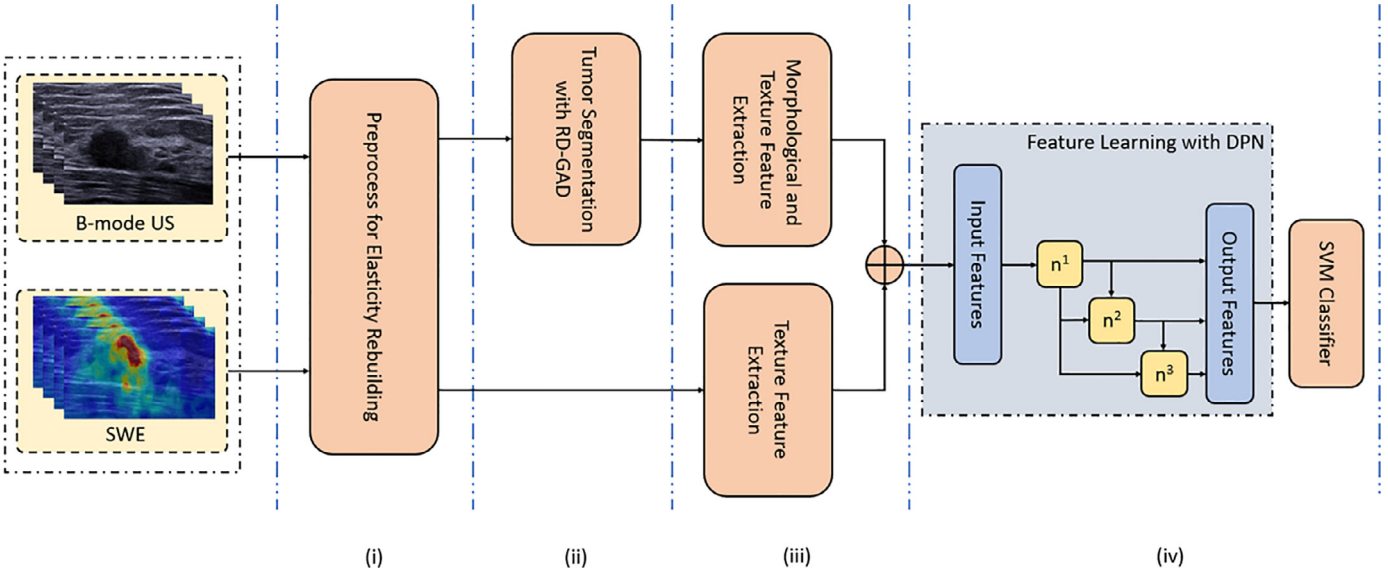

Fig. 1. Flowchart of the proposed deep polynomial network (DPN) method on dual-modal ultrasound for breast tumor diagnosis. (i) Image preprocessing. (ii) Tumor segmentation. (iii) Dual-modal feature extraction. (iv) Feature learning and classification with DPN; here, n^i represents layers of nodes.

The diagnosis of breast tumors with ultrasound often relies on visual interpretation of ultrasound images by experienced radiologists, which is subjective, time-consuming, tedious, and also limits the diagnosis accuracy. Thus, it is desirable to develop approaches using artificial intelligence (AI) for more objectively, accurately, and efficiently interpreting dual-modal ultrasound images and distinguishing between malignant and benign breast tumors [7]. In this paper, we have proposed an AI-based architecture for breast tumor classification on dual-modal ultrasound. The contributions of this work are two-fold: (i) Contourlet-based texture features and morphological features have been extracted from dual-modal ultrasound images, following an improved tumor segmentation model with the reaction diffusion (RD) level set. (ii) Dual-modal features have been combined by using a deep learning method called the deep polynomial network (DPN) to facilitate feature learning and to yield accurate classification of breast tumors. To the best of our knowledge, this study is among the first to propose an AI-based architecture on dual-modal ultrasound namely SWE and B-mode for breast cancer diagnosis.

2. Materials and methods

Our methods were comprised of four steps as show in Figure 1. First, the dual-modal ultrasound images were preprocessed to be suitable for following analysis. Second, tumor segmentation was conducted on B-mode images with the reaction diffusion (RD) level set model combined with the Gabor-based anisotropic diffusion (GAD) algorithm, named RD-GAD, and then the segmented tumors locations were mapped back to the paired SWE images. Third, 82 quantitative features were extracted from B-mode and SWE images, including morphological features and contourlet-based texture features. Fourth, the deep polynomial network was utilized to facilitate learning and to improve tumor classification by combining the dual-modal features and constructing a new set of features that were more informative and discriminating than the initial features.

2.1. Dual-modal image acquisition and preprocessing

This was a retrospective study approved by the Institutional Review Board and informed consent of all patients was obtained. The study group consisted of patients with visible breast abnormalities on routine B-mode scans. A total of 227 dual-modal images with both SWE and B-mode were acquired from 121 women, consisting of 135 images of benign tumors and 92 of malignant tumors. Pathology served as the gold standard for diagnosis. The ultrasound examination was conducted with the Aixplorer system (Supersonic Imagine, Aix-en-Provence, France) equipped with a 4–15 MHz linear array broadband probe. The SWE and B-mode images were displayed on the monitor simultaneously, with the SWE on the top and the B-mode image on the bottom (Fig. 2(a)).

The SWE image was displayed as a composite color image, which was a transparent color image named the pure SWE image superimposed on the background of the grayscale B-mode image (Fig. 2(b)). With an in-house software, the color SWE was converted into a grayscale image of elastic modulus to rebuild its elasticity information of tissues as follows [10]. First, the pure SWE image (Fig. 2(d)) was derived by subtracting the B-mode grayscale image (Fig. 2(c)) from the composite SWE image (Fig. 2(b)). Then each pixel on the pure SWE image was compared with all colors in the color bar displayed to the right of the dual-modal image (Fig. 2(a)) to find its closest color and rebuild the corresponding elasticity modulus value [10]. After pixel-by-pixel rebuilding, the pure SWE image was transformed to a grayscale elastographic image (Fig. 2(e)).

2.2. Breast tumor segmentation

The lesion boundaries are usually not obvious in the elastograms of breast tumors. In order to detect the locations of breast tumors, the boundaries of tumors were automatically delineated on the B-mode images with our improved reaction diffusion (RD) level set model, namely RD-GAD. The tumor boundaries detected on B-mode images were then mapped to SWE images. The RD-GAD model for segmentation of B-mode images is presented as follows.

Firstly, the GAD was used for suppression of speckle noise on an ultrasound image I and preservation of tissue edges so as to construct the stopping edge function g for the level set segmentation [11].

$$g = \frac{1}{1 + |\nabla \mathrm{GAD}(I)|^2} \tag{1}$$

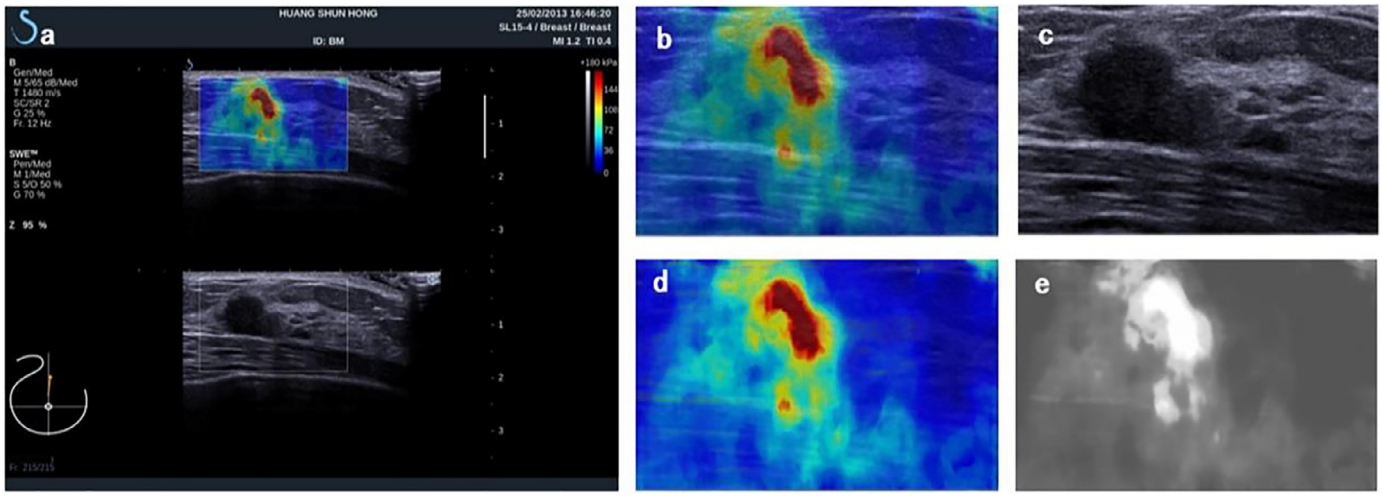

Fig. 2. Dual-modal display of an SWE image and a B-mode image for a breast tumor and the elasticity rebuilding. (a) Dual-model images with the composite SWE image on the top and the grayscale B-mode image on the bottom; (b) the composite SWE image; (c) the B-mode image; (d) the pure SWE image; (e) the elastographic image shown in grayscales rebuilt from the RGB color space.

where ∇ was the gradient operator, and GAD(I) was the ultrasound image filtered with the GAD.

Then the function g was integrated into the evolution equation of the RD level set, for controlling the curve evolution to stop at the desired boundaries of breast tumors. The evolution equation of the RD-GAD was given by

$$\begin{cases} \varphi_t == \varepsilon\Delta\varphi - \dfrac{1}{\varepsilon}[L(\varphi) + \alpha \cdot g \cdot \delta(\varphi)] \\ \text{subject to } \varphi(x, t = 0, \varepsilon) = \varphi_0(x) \end{cases} \tag{2}$$

where ε was a small positive constant; Δ was the Laplacian operator; ϕ was the level set function; ϕ_0 was an initial level set function; $\delta(\cdot)$ was the Dirac function; α was the coefficient that controlled the weight of the stopping edge function.

In this paper, we used the true positive rate (TPR_S), false positive rate (FPR_S), accuracy (ACC_S), specificity (SPE_S), and root mean square error (RMSE) as the quantitative indices to evaluate the segmentation performance of the RD-GAD model, with the manual segmentation results as the gold standard [12]. The subscript "_S" means these indices were used for assessing the tumor segmentation rather than the terminal task namely tumor classification. The three indices TPR_S, ACC_S, and SPE_S measure the similarity and overlap between the region segmented by an algorithm and the gold standard region, and their values are between 0 and 1. The larger the values are, the more accurate the segmentation is [13]. The RMSE reflects the average distance between the tumor contour detected by an algorithm and the gold standard contour. The smaller the value, the more accurate the segmentation [13].

2.3. Feature extraction

Morphological and texture features of breast tumors were extracted as follows. Ten morphological features describing the structure, shape and size of a breast tumor were computed from the B-mode images including the area, convex area, convex area ratio, rectangular area ratio, perimeter, diameter, long- and short-axis lengths, orientation and eccentricity [14].

Seventy-two contourlet-based texture features were calculated on the bandpass bands decomposed from the SWE and B-mode images by using the contourlet transform [10], where 36 were from one modality. These texture features were extracted from the segmented area of a breast tumor, including: (i) five features computed on the binary images after the adaptive thresholding algorithm, namely the area ratio, center deviation degree, dispersion degree, radial deviation degree, and combined area ratio [15]; (ii) eleven first-order statistical features of the intensities [14], including the mean, standard deviation, maximum, minimum, median, third quartile, coefficient of variance, skewness, kurtosis, entropy of the histogram and entropy of the brightness; (iii) twenty features calculated with the gray level co-occurrence matrix (GLCM), i.e. the contrast, correlation, energy, homogeneity, and entropy [10,14,15]. In our practice, the GLCM was computed at distances of 1, 2, 3, and 4 pixels and directions of 0°, 45°, 90° and 135°, and the GLCM features were averaged over four directions [15]. For methodological details of contourlet-based texture feature extraction, readers can refer to our previous publication [10].

2.4. Feature learning with deep polynomial networks

Deep polynomial networks are deep neural networks where the output of each node is a quadratic function of its inputs [16]. DPNs learn polynomial predictors by a deep network architecture that provides a good approximate basis for the values attained by polynomials over the training samples. The DPN is suitable for small data samples and has high computational efficiency [17]. Here, we used the DPN to construct a new set of dual-modal ultrasound features that were more informative and discriminating than the initial features for breast tumor classification.

When constructing the first layer in DPNs, the set of values by degree-1 polynomial (linear) function over training samples was given by Livni et al. [18]

$$\left\{(\langle w, [1x_1]\rangle, \cdots, \langle w, [1x_m]\rangle) : w \in \mathrm{R}^{d+1}\right\}, \tag{3}$$

which was the $(d+1)$-dimensional linear subspace of $\mathbf{R}^m$. Here, $\langle \bullet, \bullet \rangle$ was the inner product. To simplify the model, we specified the linear transformation by a matrix W which mapped $[\mathbf{1}\ X]$ into the constructed basis, where $\mathbf{1}$ was the all-ones vector, and X was a matrix of samples $X = [\boldsymbol{x}_1, \boldsymbol{x}_2, \ldots, \boldsymbol{x}_m]$. The columns of W, denoted by $\boldsymbol{w}_j$, $j = 1, \ldots, d+1$, meant the $d+1$ linear functions forming the first layer in the DPN; namely, the jth node of the first layer was the function

$$n_j^1(x) = \left\langle \boldsymbol{w}_j,\ [\mathbf{1}\ X] \right\rangle \tag{4}$$

Here, $\{(\mathrm{n}_\mathrm{j}^1(\boldsymbol{x}_1),\ \ldots,\ \mathrm{n}_\mathrm{j}^1(\boldsymbol{x}_\mathrm{m}))\}_{\mathrm{j}=1}^{\mathrm{d}+1}$ was a basis for all values obtained by degree-1 polynomials over training samples. Let F^1 be an $m \times (d+1)$ matrix with $\mathrm{F}_{\mathrm{i,j}}^1 = \mathrm{n}_\mathrm{j}^1(\mathrm{x}_\mathrm{i})$.

We then performed an iteration process to evolve a matrix F. We initialized F as an empty matrix. At the first iteration ($t=1$), $F:=F^1$. At the following iterations ($t>1$), the matrix F was maintained, whose columns formed a basis for the values attained by all polynomials of degree $\leq(t-1)$. That is to say, we found a column subset F^t so that the columns of [F F^t] formed a basis for the columns of [F $\tilde{F}^t$], where

$$\tilde{F}^t = \left[\left(F_1^{t-1}\circ F_1^1\right)\cdots\left(F_1^{t-1}\circ F_{|F_1|}^1\right)\cdots\left(F_{|F^{t-1}|}^{t-1}\circ F_1^1\right)\cdots \left(F_{|F^{t-1}|}^{t-1}\circ F_{|F_1|}^1\right)\right] \quad (5)$$

Then F was redefined as an augmented matrix $F:=[F\ F^t]$, $t=2$, 3, ….

For achieving the balance between simplicity and accuracy in practice, we adopted the following strategy to quickly decrease the training error by using a small number of nodes in a computationally cheap way [18]. We computed a linear transformation at the first layer which transformed the augmented data matrix [**1** X] into its leading singular vectors. The next layers used a standard orthogonal least squares approach for greedily picking the columns of $\tilde{F}^t$ that were most relevant for prediction [19]. We iteratively picked the column of $\tilde{F}^t$ whose residual after projecting on the existing basis F was most correlated with the residual of the labels $\boldsymbol{y}$, also after projecting on the existing basis F. The column was then added to the existing basis, and the process repeated itself.

After feature learning on the initial dual-modal ultrasound features with the DPN, the output of the network was the basis F, which was a new set of features combining SWE and B-mode characteristics and were supposed to be more informative and discriminating than the initial features. We then utilized a support vector machine (SVM) on F for classification between malignant and benign breast tumors.

In this work, the depth of the DPN model was set to 3 (excluding the input and output layers), and the number of nodes at each layer was set to 30. The quantitative indices for classification evaluation were sensitivity (SEN), specificity (SPE), accuracy (ACC), Youden's index (YI), and area under the receiver operating characteristic curve (AUC) [14].

3. Results

3.1. Results of tumor segmentation

The proposed segmentation model RD-GAD was based on the RD algorithm and we compared the RD-GAD with the traditional RD for breast tumor segmentation.

Figure 3(a)–(d) shows segmentation results for a benign breast tumor. The border of the breast tumor was uncontinuous and broken at 4 to 5 o'clock. The RD-GAD model extracted the broken edges more effectively and accurately than the traditional RD method, and its segmentation result was more close to the result of the manual segmentation. Figure 3(e)–(h) shows segmentation results of a malignant breast tumor with a relatively complex shape and uneven edges. Compared with the traditional RD method, the RD-GAD algorithm more effectively extracted the convex and broken edges at 8 o'clock, which was more consistent with the result of the manual segmentation.

To compare performance of the RD-GAD with traditional RD method quantitatively, we used the two models to segment 227 ultrasound images of breast tumors. From Table 1, the RD-GAD algorithm was superior to the traditional RD algorithm in terms of ACC_S, TPR_S and RMSE. The ACC_S values of the RD and RD-GAD were 95.6% ± 4.6% and 96.3% ± 4.7%, the TPR_S values were 79.3% ± 10.8% and 86.7% ± 7.70%, and the RMSE values were 8.53 ± 7.83 pixel and 7.27 ± 7.98 pixel, respectively. It was also shown that the FPR_S of the RD-GAD (7.6% ± 19.4%) was close to that of the RD (4.6% ± 16.9%), both maintained at low values. Taking all the indices into consideration, it was demonstrated that the RD-GAD algorithm was better than the traditional RD algorithm for the segmentation of ultrasound images.

Table 1
The quantitative indices of breast ultrasound image segmentation.

Indices		TPR_S	FPR_S	ACC_S	RMSE/pixel
RD	Mean	0.793	0.046	0.956	8.528
	Std	0.108	0.169	0.046	7.829
RD-GAD	Mean	0.867	0.076	0.963	7.266
	Std	0.077	0.194	0.047	7.976

Table 2
Single-modal classification results.

	B-model				SWE			
	PCA		DPN		PCA		DPN	
	ORIG	CONT	ORIG	CONT	ORIG	CONT	ORIG	CONT
SEN	63.0%	63.0%	98.9%	94.6%	75.0%	76.1%	96.7%	96.7%
SPE	77.0%	79.3%	85.9%	82.2%	89.6%	88.9%	91.1%	88.9%
ACC	71.4%	72.7%	91.2%	87.2%	83.7%	83.7%	93.4%	92.1%
YI	40.1%	42.3%	84.8%	76.8%	64.6%	65.0%	87.9%	85.6%
AUC	0.730	0.732	0.864	0.837	0.882	0.908	0.920	0.934

3.2. Results of classification

In addition, the principal component analysis (PCA) model, the multiple kernel learning (MKL) model and the DPN model were compared for feature learning. Pertaining to the PCA method, the dual-modal features were concatenated as the input of the PCA. The feature dimension contributing to the variance more than 95% was reserved [20]. Pertaining to the MKL method, features extracted from SWE and B-mode ultrasound were fused as follows. First, two types of features of different modalities were trained to obtain two kernel functions. Then these two kernel functions were combined into a kernel function. Finally, the classifier used this fused kernel function to classify the breast tumors [21].

3.2.1. Single modal classification results

The classification performance of the PCA model and DPN model for a single modality was calculated. In order to compare the contourlet-based texture features (at the contourlet [CONT] domain) with the texture features extract from the raw images (at the original [ORIG] domain), we also used the PCA model and MKL model for classification of breast tumors at these two different domains. As shown in Table 2, for the B-mode alone, at the ORIG domain, the DPN model achieved the best classification SEN, SPE, ACC, YI, and AUC in a validation set via the leave-one-out cross-validation, which reached 98.9%, 85.9%, 91.2%, 84.8%, and 0.864, respectively. For the SWE alone, at the ORIG domain, the DPN model also achieved the best classification indices with the leave-one-out cross validation, which reached 96.7%, 91.1%, 93.4%, 87.9%, and 0.920, respectively. The results indicated that the DPN model performed better than the PCA model for a single modality.

3.2.2. Dual-modal classification results

The classification results at different domains of dual-modal features are listed in Table 3. The DPN model at the CONT domain achieved an SPE of 94.1%, an ACC of 95.6%, a YI of 91.9% and an AUC of 0.961, respectively, which were increased by 2.2%, 1.3%, 2.2%, and 0.037, respectively, compared to its counterparts at the ORIG domain. At the CONT domain, the PCA model achieved an SEN of 85.9%, an ACC of 85.9%, a YI of 71.8% and an AUC of

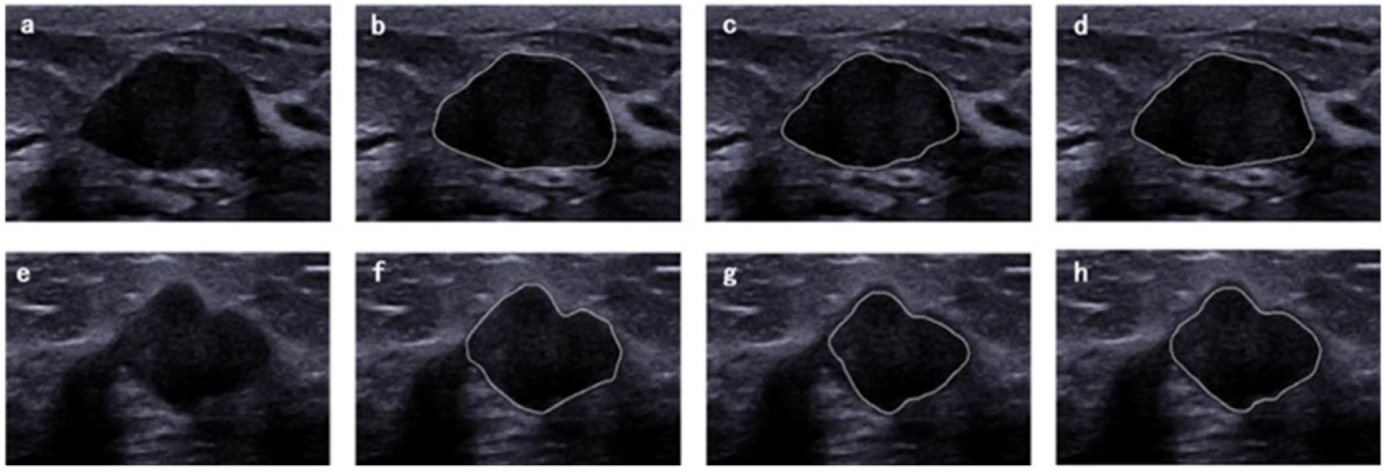

Fig. 3. Segmentation results of a benign breast tumor (a–d) and a malignant breast tumor (e–h). (a, e) The B-mode ultrasound images; (b, f) results of manual segmentation by radiologists, as the gold standard for segmentation; (c, g) results of the traditional RD model; (d, h) results of the RD-GAD model.

Table 3
Dual-modal classification results.

	ORIG			CONT		
	PCA	MKL	DPN	PCA	MKL	DPN
SEN	80.4%	73.9%	97.8%	85.9%	75.0%	97.8%
SPE	88.1%	86.7%	91.9%	85.9%	90.4%	94.1%
ACC	85.0%	81.5%	94.3%	85.9%	84.1%	95.6%
YI	68.6%	60.6%	89.7%	71.8%	65.4%	91.9%
AUC	0.880	0.871	0.924	0.908	0.915	0.961

0.908, respectively, with the leave-one-out cross validation, which were increased by 5.5%, 0.9%, 3.2% and 0.028, respectively, compared to the results at the ORIG domain. The MKL model at the CONT domain achieved an SEN of 75.0%, an SPE of 90.4%, an ACC of 84.1%, a YI of 65.4% and an AUC of 0.915, respectively, which were increased by 1.1%, 3.7%, 2.6%, 4.8% and 0.044, respectively, compared to its counterparts at the ORIG domain. The experimental results showed that the contourlet-based texture features had superior performance to the traditional features for tumor diagnosis with dual-modal ultrasound images.

It was also seen from Table 3 that the SEN (97.8%), SPE (94.1%), ACC (95.6%), YI (91.9%), and AUC (0.961) of the dual-modal DPN method at the CONT domain were increased by 1.1%, 3%, 2.2%, 4%, and 0.041, respectively, compared to the best classification results of the single-model DPN methods. The SEN (85.9%), ACC (85.9%) and YI (71.8%) of the dual-modal PCA method at the CONT domain were increased by 9.8%, 2.2% and 6.8%, respectively compared to the best classification results of the single-model PCA methods. These results showed that the methods with dual-modal features outperformed their counterparts with single-modal features. It also indicated that dual-modal features could more comprehensively express and capture the information of benign and malignant breast tumors than single-modal features, thus elevating the accuracy of the artificially intelligent diagnosis.

As enumerated in Tables 2 and 3, the DPN model at the CONT domain achieved the best SEN of 97.8%, SPE of 94.1%, ACC of 95.6%, YI of 91.9%, and AUC of 0.961 in the validation set, respectively. Compared to all other classification models, the best classification performance was improved by 11.9%, 8.2%, 9.7%, 20.1%, and 0.053, respectively. These results indicated that the DPN model could more effectively learn the relationships between features of different modalities and thus it could help to more accurately classify breast tumors.

Table 4
Classification performance in representative publications.

Literature	Patient no.	Tumor no.	Method	SEN (%)	SPE (%)	ACC (%)	YI (%)	AUC
Zhang et al. [31]	121	227	S	88.6	97.1	93.4	85.7	0.947
Wang et al. [32]	100	126	S	93.4	95.4	94.4	88.8	0.952
Moon et al. [22]	106	109	B + S	90.4	94.7	92.3	85.1	0.961
Han et al. [33]	5151	7408	B	86.0	96.0	90.0	82.0	0.900
Yu et al. [34]	187	137	S	95.1	94.6	94.8	89.7	–
Song et al. [35]	200	209	B + S	68.2	98.0	82.8	66.2	–
This study	121	227	B + S	97.8	94.1	95.6	91.9	0.961

S = quantitative features on shear-wave elastography; B = quantitative features on B-mode ultrasound.
This study and [31,33,34] were performed with cross-validation.

4. Discussion

The most important contribution of this work is the introduction of AI architecture to breast cancer diagnosis with dual-modal ultrasound. This study used a deep learning algorithm, the DPN, to achieve more accurate, efficient and convenient classification. The dual-modal AI architecture was superior to all other compared methods and could improve the classification performance of breast tumors, which indicated that the AI-based technique could get close results to breast tumor biopsies and could be potentially applied to clinical non-invasive diagnosis.

Our dual-modal DPN method achieved superior or comparative performance compared to various recent studies outlined in Table 4. The AUCs across these studies ranged from 0.900 to 0.961, the YIs were between 66.2% and 91.9%, and the ACCs were between 82.8% and 95.6%. Our method yielded the largest AUC (0.961), the largest ACC (95.6%) and the largest YI (91.9%), demonstrating that our AI-based method has the state-of-the-art classification ability. The two studies with the largest AUCs (ours and [22]) were both based on dual-modal features, indicating that the dual-modal methods outperformed the single-modal methods for classification of breast tumors. The dual-modal methods could more fully capture the benign and malignant information from breast tumors and thus could elevate diagnostic performance [23].

In this paper, we proposed an improved RD method for tumor segmentation, i.e., the RD-GAD. The RD method is a level set model that is free of the costly reinitialization procedure and has been proved to be valuable in image segmentation [24,25]. However, the traditional RD model cannot be directly applied to medical ultrasound images, because the speckle noise, an inherent,

multiplicative noise in ultrasonic imaging, largely blurs the image details and reduces the contrast of the image. We combined the RD model with the GAD algorithm in order to suppress the effect of speckle noise on segmentation and thus made the RD-GAD capable of accurately segmenting B-mode ultrasound images.

At present, morphological features on ultrasound are generally used in artificially intelligent diagnosis systems for breast tumors [26]. To augment the classification accuracy of the AI-based systems, we extracted texture features from tumors by using the contourlet transform. The contourlet transform quantified textures that represented tumor elastic heterogeneity on spatial-frequency domain, bringing detailed information to tumor classification [10]. The combination of the morphological features and texture features improved the accuracy for breast tumor classification.

There are some limitations and directions for future work. First, the RD-GAD algorithm rendered automated segmentation of breast lesions and helped diagnose breast tumors. With more advanced machine learning especially deep learning approaches [26–29], the segmentation accuracies are expected to be further enhanced. Second, we combined features from SWE and B-mode for dual-modal classification by using the DPN algorithm. Only one type of elastography, i.e., SWE [30], was adopted, and other types such as strain elastography could be integrated for ultrasonic multimodal diagnosis in the future. Third, the parameters in the DPN algorithm such as the node number and depth were emperically adjusted to yield the best performance. It is important to explore a more intelligent and effective approach for the optimal parameter setting.

5. Conclusion

In conclusion, we propose a dual-modal AI-based framework for diagnosis of breast tumors. The experimental results show that the dual-modal DPN was superior to all other frameworks, indicating that the AI architecture can assist in more effective and more convenient classification of breast tumors.

Conflict interest

There is no conflict of interest.

Ethical approval

This was a retrospective study approved by the Institutional Review Board and informed consent of all patients was obtained.

Acknowledgments

The work was funded by the National Science Foundation of China (Nos. 61671281, 81627804, and 61471231).

References

[1] World Health Organization Breast cancer: prevention and control. World Health Stat Ann 2012;41:697–700.
[2] Wooster R, Bignell G, Lancaster J, Swift S, Seal S, Mangion J, Collins N, Gregory S, Gumbs C, Micklem G. Identification of the breast cancer susceptibility gene BRCA2. Nature 2015;378:789.
[3] Ciatto S, Cecchini S, Iossa A, Grazzini G. T category and operable breast cancer prognosis. Tumori 2015;75:18–22.
[4] Pantanowitz L, Sinard JH, Henricks WH, Fatheree LA, Carter AB, Contis L, Beckwith BA, Evans AJ, Lal A, Parwani AV. Validating whole slide imaging for diagnostic purposes in pathology: guideline from the College of American Pathologists Pathology and Laboratory Quality Center. Arch Pathol Laborat Med 2013;137:1710.
[5] Guo R, Lu G, Qin B, Fei B. Ultrasound imaging technologies for breast cancer detection and management: a review. Ultrasound Med Biol 2017;44:37–70.
[6] Pardini B, Naccarati A, Novotny J, Smerhovsky Z, Vodickova L, Polakova V, Hanova M, Slyskova J, Tulupova E, Kumar R. DNA repair genetic polymorphisms and risk of colorectal cancer in the Czech Republic. Mutat Res Fund Mol Mech Mutag 2008;638:146.
[7] Huang Q, Huang X, Liu L, Lin Y, Long X, Li X. A case-oriented web-based training system for breast cancer diagnosis. Comput Methods Progr Biomed 2018;156:73.
[8] Barr RG, Nakashima K, Amy D, Cosgrove D, Farrokh A, Schafer F, Bamber JC, Castera L, Choi BI, Chou YH. WFUMB guidelines and recommendations for clinical use of ultrasound elastography: Part 2: breast. Ultrasound Med Biol 2015;41:1148–60.
[9] Zhang Q, Suo J, Chang W, Shi J, Chen M. Dual-modal computer-assisted evaluation of axillary lymph node metastasis in breast cancer patients on both real-time elastography and B-mode ultrasound. Eur J Radiol 2017;95:66–74.
[10] Zhang Q, Xiao Y, Chen S, Wang C, Zheng H. Quantification of elastic heterogeneity using contourlet-based texture analysis in shear-wave elastography for breast tumor classification. Ultrasound Med Biol 2015;41:588–600.
[11] Chan TF, Vese LA. Active contours without edges. IEEE Press; 2001.
[12] Zheng W, Kim JP, Kadbi M, Movsas B, Chetty IJ, Glide-Hurst CK. Magnetic resonance-based automatic air segmentation for generation of synthetic computed tomography scans in the head region. Int J Rad Oncol Biol Phys 2015;93:497–506.
[13] Bai X, Cao Z, Wang Y, Yu Z, Hu Z, Zhang X, Li C. Vegetation segmentation robust to illumination variations based on clustering and morphology modelling. Biosyst Eng 2014;125:80–97.
[14] Zhang Q, Xiao Y, Suo J, Shi J, Yu J, Guo Y, Wang Y, Zheng H. Sonoelastomics for breast tumor classification: a radiomics approach with clustering-based feature selection on sonoelastography. Ultrasound Med Biol 2017;43:1058.
[15] Zhang Q, Li C, Han H, Yang L, Wang Y, Wang W. Computer-aided quantification of contrast agent spatial distribution within atherosclerotic plaque in contrast-enhanced ultrasound image sequences. Biomed Signal Process Control 2014;13:50–61.
[16] Shi J, Zhou S, Liu X, Zhang Q, Lu M, Wang T. Stacked deep polynomial network based representation learning for tumor classification with small ultrasound image dataset. Neurocomputing 2016;194:87–94.
[17] Shi J, Qian Y, Wu J, Zhou S, Cai Y, Zhang Q, Feng X, Chang C. Ultrasound image based tumor classification via deep polynomial network and multiple kernel learning. Curr Med Imag Rev 2018;14:301–8.
[18] Livni R, Shalevshwartz S, Shamir O. An algorithm for training polynomial networks. Comput Sci 2013;26:4748–50.
[19] Chen S, Billings SA, Luo W. Orthogonal least squares methods and their application to non-linear system identification. Int J Control 1989;50:1873–96.
[20] Virmani J, Dey N, Kumar V, PCA-PNN and PCA-SVM based CAD systems for breast density classification, 96, 159–180 (2016).
[21] Shen H, Kai D, Böcker S, Rousu J. Metabolite identification through multiple kernel learning on fragmentation trees. Bioinformatics 2014;30:157 i.
[22] Moon WK, Huang YS, Lee YW, Chang SC, Lo CM, Yang MC, Bae MS, Lee SH, Chang JM, Huang CS. Computer-aided tumor diagnosis using shear wave breast elastography. Ultrasonics 2017;78:125–33.
[23] Turgut E, Celenk C, Tanrivermis SA, Bekci T, Gunbey HP, Aslan K. Efficiency of B-mode ultrasound and strain elastography in differentiating between benign and malignant cervical lymph nodes. Ultrasound Q 2017;33:201.
[24] Zhang Q, Han H, Ji C, Yu J, Wang Y, Wang W. Gabor-based anisotropic diffusion for speckle noise reduction in medical ultrasonography. J Opt Soc Am A Opt Image Sci Vis 2014;31:1273–83.
[25] Tsiotsios C, Petrou M. On the choice of the parameters for anisotropic diffusion in image processing. Pattern Recogn 2013;46:1369–81.
[26] Huang Q, Zhang F, Li X. Machine learning in ultrasound computer-aided diagnostic systems: a survey. Biomed Res Int 2018;2018:1–10.
[27] Yang X, Yu L, Li S, Wen H, Luo D, Bian C, Qin J, Ni D, Heng PA. Towards automated semantic segmentation in prenatal volumetric ultrasound. IEEE Trans Med Imag 2018;99. doi:10.1109/TMI.2018.2858779.
[28] Wang Y, Deng Z, Hu X, Zhu L, Yang X, Xu X, Heng P-A, Ni D. Deep attentional features for prostate segmentation in ultrasound. In: Proc Med Image Comput Comput Assist Interv (MICCAI). Cham, Switzerland: Springer; 2018. p. 523–30.
[29] Yang X, Yu L, Wu L, Wang Y, Ni D, Qin J, Heng PA. Fine-grained recurrent neural networks for automatic prostate segmentation in ultrasound images. In: Proc. AAAI Conf Artificial Intelligence. Palo Alto, California: AAAI Press; 2016. p. 1633–9.
[30] Zhou BG, Wang D, Ren WW, Li XL, He YP, Liu BJ, Wang Q, Chen SG, Alizad A, Xu HX. Value of shear wave arrival time contour display in shear wave elastography for breast masses diagnosis. Sci Rep 2017;7:7036.
[31] Zhang Q, Xiao Y, Dai W, Suo J, Wang C, Shi J, Zheng H. Deep learning based classification of breast tumors with shear-wave elastography. Ultrasonics 2016;72:150–7.
[32] Wang M, Yang Z, Liu C, Yan J, Zhang W, Sun J, Cui G. Differential diagnosis of breast category 3 and 4 nodules through BI-RADS classification in conjunction with shear wave elastography. Ultrasound Med Biol 2016;43:601–6.
[33] Han S, Kang HK, Jeong JY, Park MH, Kim W, Bang WC, Seong YK. A deep learning framework for supporting the classification of breast lesions in ultrasound images. Phys Med Biol 2017;62:7714–28.
[34] Yu Y, Xiao Y, Cheng J, Chiu B. Breast lesion classification based on supersonic shear-wave elastography and automated lesion segmentation from B-mode ultrasound images. Comput Biol Med 2017;93:31.
[35] Song EJ, Sohn YM, Seo M. Diagnostic performances of shear-wave elastography and B-mode ultrasound to differentiate benign and malignant breast lesions: the emphasis on the cutoff value of qualitative and quantitative parameters. Clin Imag 2018;50:302–7.